AIAA JOURNAL
Vol. 48, No. 12, December 2010

Shock—Water Column Interaction, from Initial Impact to Fragmentation Onset

D. Igra* and M. Sun†
Tohoku University, Sendai 980-8578, Japan

DOI: 10.2514/1.44901

A numerical study of shock wave loading on a cylindrical water column using a new scheme is presented. This scheme can capture gas–liquid interfaces sharply without introducing density diffusion or pressure oscillations. In addition, it can resolve fragments smaller than 1 grid-cell size. Results obtained by employing this new numerical scheme agree well with experimental findings for the water column deformation when hit by planar shock waves for which the Mach numbers were 1.3 and 1.47. In addition, it was possible to observe the onset of fragmentation of the water column, which was positioned at the same location as was done in previous experimental results. In previously published computational fluid dynamics works, only the initial impact of the shock wave with the water column was simulated; therefore, deformation was usually not considered. Finally, results obtained for a Mach 3 shock wave interaction with a water column are discussed. In all results obtained during the current work, stripping breakup occurs, and it was possible to observe the onset of fragmentation. No Rayleigh–Taylor-type oscillations were observed in any cases presented in the current research.

Nomenclature

d	=	droplet diameter
d_0	=	initial water column diameter
M	=	Mach number
t	=	time elapsed from shock wave impingement
t^*	=	nondimensional time
U	=	velocity difference between gas and droplet
u_2	=	induced flow velocity behind shock wave
W_e	=	Weber number
γ	=	specific heat ratio
ρ	=	density
σ	=	surface tension

I. Introduction

THE breaking of liquid droplets due to the high-speed flow around them has many applications in fluid mechanics and was, therefore, investigated by many researchers. A comprehensive review of droplet breakup was given by Wierzba and Takayama [1], in which several breakup modes were discussed. One of the more common modes that occurs when liquid droplets are impinged by shock waves is the so-called stripping-type breakup. It takes place over a wide range of Weber numbers ranging, approximately, from 100 to 20,000 [1]. The Weber number We is defined as $We = \rho U^2 d/\sigma$, where ρ is the gas density, U is the velocity difference between the gas and the droplet, d is the droplet diameter, and σ is the surface tension. In the following, a brief description of previous experimental work is given; thereafter, the current computational fluid dynamics (CFD) status of shock wave interaction with liquid drops is discussed.

Some of the early experimental investigations regarding stripping-type breakup have been conducted by Ranger and Nicholls [2,3]. They studied the shock wave/liquid-droplet interaction at various stages of the breakup processes using streak photography. Recently Joseph et al. [4] conducted similar experiments using a high-speed camera. Their results were concluded from a series of experiments in which various liquids were used. The incident shock waves of Mach numbers in their experiments were two and three. Only the shock wave interaction with a liquid droplet and the waves generated around the droplet were observed. Other experiments regarding the stripping-type breakup were conducted by Hirahara and Kawahashi [5], Krzeczkowski [6], Simpkins and Bales [7], Yoshida and Takayama [8], and Theofanous and Li [9].

Yoshida and Takayama [8] showed that different droplet breakup patterns are observed when using different methods for flow visualization. The patterns of droplet disintegration observed while using double-exposure image holographic interferometry were different from those observed on unreconstructed holograms that were essentially equivalent to a direct shadowgraph.

However, most of the recorded experiments used schlieren or shadowgraph methods for visualizing the droplet breakup process. In these results, the shapes of the disintegrating spherical droplets resembled fireballs (Ranger and Nicholls [2], Joseph et al. [4], and Simpkins and Bales [7]). Based on these photographs, the internal structure of the disintegrating spherical droplets, such as shattering mist clouds and wakes, were hardly distinguished. On the other hand, when using holographic interferometry, the obtained (slightly three-dimensional) images showed mist clouds and wakes that were different from those observed in schlieren and shadowgraph photographs. The object beams of holographic interferometry carry phase information created by the light scattered from the micromist particles to the holofilm. Through the process of reconstruction, the phase information was partially recovered, whereas in the schlieren or shadowgraph methods, this information could not be captured.

Wierzba and Takayama [10] examined in detail the stripping-type breakup of water droplets and concluded that the breakup process could be divided into four stages. Their images were clear enough to view the structure of the droplet during the various deformation stages of the breakup process. Recently, the experimental results of Theofanous and Li [9] achieved similar quality results. In both cases, the frontal part of the droplet looked to be a smooth and round surface; no surface waves were visible.

In all experiments mentioned so far, spherical liquid droplets were employed in order to visualize the three-dimensional interaction between the oncoming shock wave and the considered droplet. However, three-dimensional visualization is still in the process of development, and wave interactions inside the droplet and the wake structure have never been correctly visualized so far. On the other

Received 13 April 2009; revision received 25 February 2010; accepted for publication 10 August 2010.

* Visiting Professor, Center for Interdisciplinary Research; currently at Rafael Advanced Defense Systems, Ltd., Department of Aeronautical Systems, Post Office Box 2250, 31021 Haifa, Israel.

† Center for Interdisciplinary Research.

hand, the interaction of a planar shock wave with a cylindrical liquid column, which is a two-dimensional droplet, can be accurately observed. To account for the process of disintegration and, particularly, to clarify the effect of wave motions inside the droplet, visualization of the head-on collision of a shock wave with a liquid column would be important. Results of such visualization could be correctly extended to interpret complex three-dimensional droplet disintegrations. Experiments with a cylindrical water column interaction with a shock wave were conducted by Igra and Takayama [11,12] for several incident shock wave Mach numbers and with different water column diameters. When comparing the deformation, it was found that the water column behaves similarly to a spherical droplet, as reported in [10]. Because of the unique experimental setup, the deformation of the water column before its complete breakup is about half of that observed in a similar spherical droplet case.

The main scope of the current work is to extend the validity of our CFD results; however, we shall first review some of the currently used CFD techniques. Water/air two-phase flows are difficult to model correctly and are one of the most challenging topics in CFD. The main problem is in modeling the interface between the gas and the liquid; this is even before we consider how a shock wave will propagate from one phase to the other. Current shock capturing schemes are generally useful in accurately simulating single-component gas flows. However, extending them to multicomponent flows having two different gases or two-phase flows often results in physically nonrealistic pressure fluctuations across the interface. These pressure fluctuations are generated as a result of deriving the pressure from the equation of state based on the total energy in gas. If we take, for example, a multicomponent flow, where the densities and velocities of the two components are initially the same, the internal energy of individual components will not be identical due to the difference in their specific heats ratios γ; hence, at every time step, energy diffusion occurs across the interface. When the value of γ changes discontinuously across the interface, an incorrect pressure value will be obtained at the interface. In the next time step, a false velocity will be derived out of the incorrect pressure values.

Many types of numerical schemes were developed in order to remedy this situation. Some common types are interface mixing-type schemes, such as those proposed by Abgrall [13] and Shyue [14]. In their schemes, the density variation at the interface was smeared due to its diffusive nature. In most of these schemes, the shock waves are typically stretched over 2–3 grid points, while the interface was smeared over 5–7 grid points. This interface mixing can only be acceptable in dealing with a pure gas phase. However, in the case of a two-phase flow consisting of gas and liquid phases, accompanied by a very large density difference between the two phases, density diffusion at the interface is strictly unacceptable. Physically interfacial mixing hardly takes place at gas/liquid interfaces, except in very special cases. Numerical diffusion might result in unphysical densities at the interfaces.

Therefore, we believe that it is advantageous to use a sharp interface between the gas and the liquid phases. In the previous works of Igra and Takayama [11,12], the cubic interpolated propagation (CIP) [15] type scheme was used: a scheme that keeps sharp interfaces. However, this is a nonconservative scheme that can result in a mass conservation error. Another approach employed by Igra and Takayama [16–18] was a level-set method [19] for interface tracking coupled with a total variation diminishing (TVD) scheme. This scheme provides better results than the CIP scheme. In both cases, only the early stage of the breakup, up to about 50 μs after the initial impact by the incident shock wave, were compared with experimental findings. The level-set method could be used for a longer time than the CIP; however, with this scheme (after some time), a problem arises in handling the water column fragmentation. This is a common problem with most interface capturing schemes, they can capture the interface correctly, but once fragmentation started, the interface breaks into parts having a size of about one cell or less; then the scheme has a serious problem in handling it. This might result in a mass conservation error. The present paper employs a recently developed scheme by Sun [20,21], which is fully conservative and can track subcell droplet fragments. This ability to handle particles smaller than the size of one computation cell is a significant improvement relative to the previously used level-set technique, as it enables computation of the droplet fragmentation initiation. Other than the papers of Igra and Takayama [15–18], very limited numerical work has been published on shock wave interaction with a water column. Nourgaliev et al. [22] used a level-set method to track the interface. Their main interest was in the shock wave motion inside the water column for about 40 μs after the initial shock wave impact. During their computation, the water column was not deformed. Other work on this subject was done by Chang and Liou [23] using the advection upstream splitting method scheme that employs a diffused interface. Their results show initial deformation of the water column but mostly thickening of the interface due to diffusion.

In the current paper, we present a comparison between our computations and experimental results that include the onset of fragmentation in the water column. In addition, we would like to demonstrate the potential of the current numerical scheme and show how it can predict the location of the initial fragmentation of the water column. Having shown these, we shall examine a higher Mach number shock wave interaction with a water column.

The present paper consists of four sections. In Sec. II, a brief review of our numerical scheme is presented. In Sec. III, the numerical scheme described in Sec. II is applied to the case of shock wave interaction with a liquid column. These numerical results are compared with experimental (interferograms) results. Finally, in Sec. IV section, conclusions from this study are drawn.

II. Numerical Scheme

In the numerical simulation, the air is assumed to be a calorically perfect gas, and water follows the Tait equation of state. In the single-phase regions, the flow is governed by the Euler equations. For the mixed cells that contain both gas and liquid phases, the cells are treated in two steps.

The first Eulerian step deals with the interactions between cells or the length scale of the grid spacing and larger. In this step, the mixed cell is approximated by the single phase with the larger volume, so that the whole flowfield is covered only by the cells with pure phases with possible material interfaces exactly aligned along the grid lines. The pressure and normal velocity at volume faces are then approximated by using an approximate Riemann solver, the Harten–Lax–van Leer–contact solver/method [24], from two neighboring pure phases. If the upstream volume has no interface, the numerical fluxes are then the same as the upwind scheme for the single-phase Euler equations. If the upstream volume has an interface inside, we have to apportion the volume of fluids to two phases. This is done by the piecewise-linear-interface-construction/volume-of-fluid (PLIC-VOF) method. The linear material interface is reconstructed in the cell according to the phase volume and its surface normals, which are given by integrating the evolution equations for surface normals. This unique PLIC-VOF technique allows the tracking of subgrid particles [21], which is essential for the simulation of defragmentation. Notice that the phase with the smaller volume in the cell does not affect the pressure and velocity, so that the small time step or the stiffness due to the small volume, known as small-cell problem, is avoided.

After conducting the Eulerian step, the pressure and the velocity of two phases in the mixed cell are, in general, not in mechanical equilibriums, which may become the source of pressure oscillations that eventually pollute numerical solutions far away. The second step, or the subgrid modeling, deals with the interactions between these two phases that are in the nonequilibrium state. These subgrid-scale interactions are modeled by two sets of Euler equations for these phases with interfaces between. The boundary conditions (continuous pressure and velocity) at the material interfaces are followed, and the model is further imposed with the periodic boundary condition, such that the resulting net flux is zero. This is similar to the step of the constrained microscale simulation in heterogeneous multiscale methods [25]. It is actually a relaxation procedure in many two-fluid models. An analytical solution has been

Table 1 Flow conditions behind the incident shock wave

Shock wave Mach number	Pressure, bar	Density, kg/m^3
1.3	1.805	1.76
1.47	2.354	2.1
3	10.33	4.48

found for the exchange of momentum, volume, and energy to the second-order accuracy for both finite and instantaneous relaxations and for general materials. For the resolved sharp interface, the subgrid modeling actually forces the two phases to develop toward the compatibility conditions between two pure phases, resulting in the same pressure and velocity in the mixed cell. It turns out that an interface with even a high-density ratio can be resolved sharply without producing nonphysical oscillations. The details of the mathematical model and numerical method are reported in a separate paper [20].

III. Numerical Results and Discussion

The numerical results presented here were obtained for three different incident shock wave Mach numbers: 1.3, 1.47, and 3. The water column diameter for the case where $M = 1.47$ is 4.8 mm, while the diameter for the other shock wave Mach numbers is 6.4 mm. In the cases where the shock wave Mach numbers were 1.3 and 1.47, a comparison between present numerical results and previous experimental findings are made and discussed. The computational domain is 150 × 150 mm, the same as the cross section of the shock tube where the experiments were conducted [11,12]. The top and bottom boundary conditions are solid walls, while the inlet and outlet are open boundaries. The low-pressure section contained air at a pressure of 1 bar and a temperature of 293 K. The flow conditions of the high-pressure section behind the shock wave are given in Table 1.

A. Results for Mach Number 1.3

In [16–18], the experimental interferograms were compared with appropriate CFD results based on a TVD scheme with a level-set method for tracking the interface. The numerical results covered a time from the initial impact and up to 55 μs after shock wave impingement on the considered water column. Here, we shall look at the flowfield at $t = 15$, 55, 105, 200, and 300 μs after the incident shock wave hits the water column. For the first two times (15 and 55 μs), the flowfield is still dominated by the impinging shock wave. In Figs. 1 and 2, density contours are shown for the flowfield at 15 and 55 μs, respectively. In both cases, the shock wave patterns in air are clearly visible. At 15 μs, the incident shock wave has almost completed its diffraction over the water column. During this time (15 μs), the reflected shock wave propagated upstream. In the water

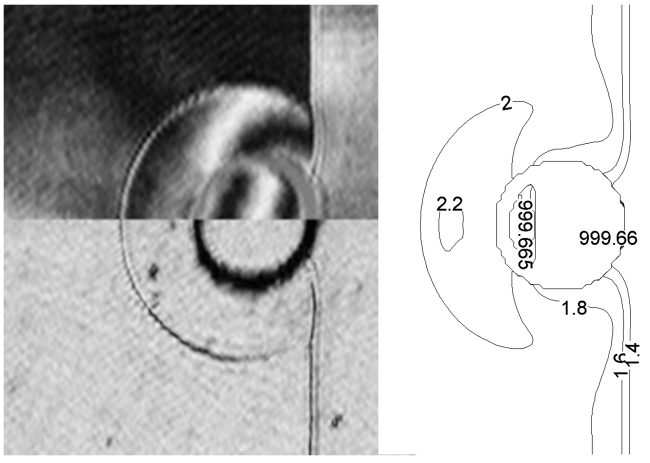

Fig. 1 Density contours (in kg/m^3) for incident shock wave Mach number 1.3 at 15 μs after impact. Experimental results taken from [17,18]: interferogram (top) and unreconstructed hologram (bottom).

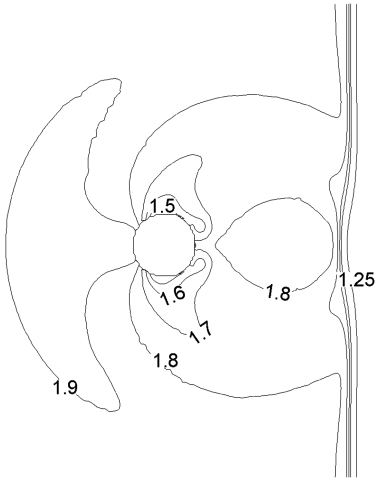

Fig. 2 Density contours (in kg/m^3) for incident shock wave Mach number 1.3 at 55 μs after impact.

column, only a minute density change is observable during this time. The water column's front half has a higher density than its rear half. This is probably due to the higher pressure exerted on the front half of the water column by the reflected shock wave and the stagnation flow

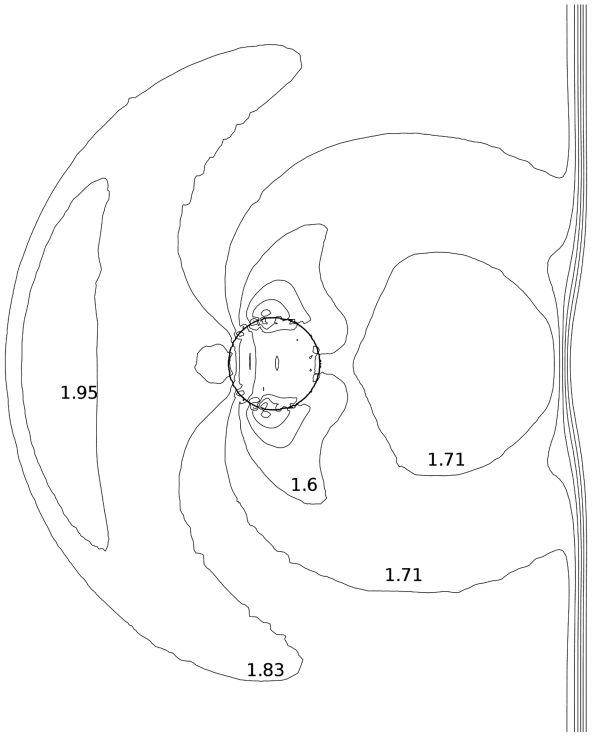

Fig. 3 Pressure contours (in bar) for incident shock wave Mach number 1.3 at 55 μs after impact.

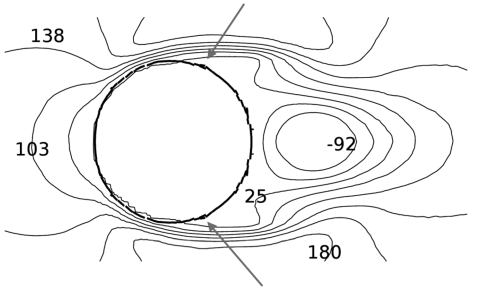

Fig. 4 Velocity contours (in m/s) in the x direction for incident shock wave Mach number 1.3 at 105 μs after impact.

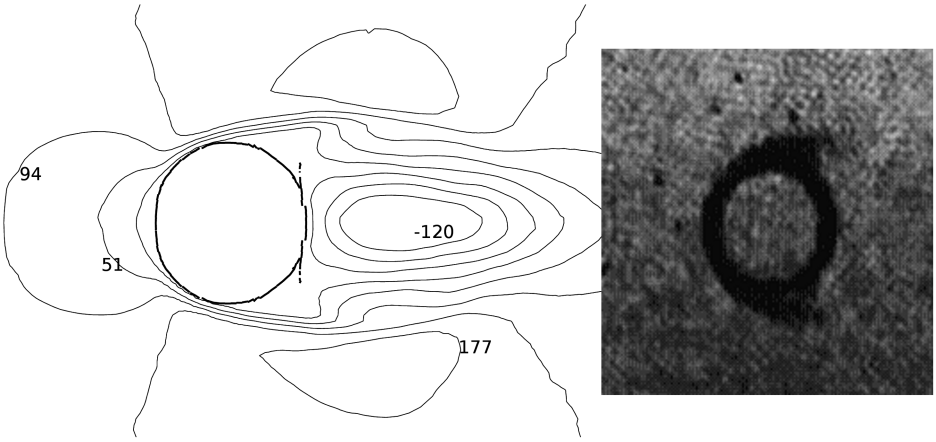

Fig. 5 Velocity contours (in m/s) in the *x* direction for incident shock wave Mach number 1.3 at 200 μs after impact. Experimental interferogram taken from [17,18].

there. The experimental interferogram from [17,18], shown next to the density contour, shows similar behavior, indicating that good agreement exists between experimental and numerical results. Looking at the next time step, at 55 μs, we can now see that a secondary reflected shock wave is present at the center of the water column. This secondary shock wave first impacted on the rear side of the water column and thereafter reflected upstream. Its initial impact created a high-pressure region at the rear of the water column, as shown in Fig. 3. In addition, the secondary shock wave (at its current location) generates relatively high-pressure regions on both sides of the water column. However, these locations are temporary and will dissipate as soon as the secondary shock wave continues its

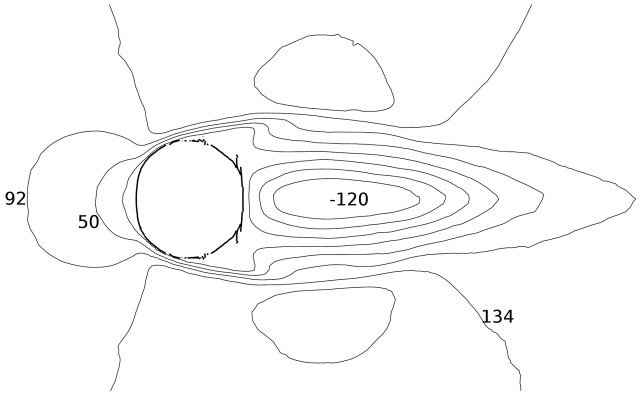

Fig. 6 Velocity contours (in m/s) in the *x* direction for incident shock wave Mach number 1.3 at 300 μs after impact.

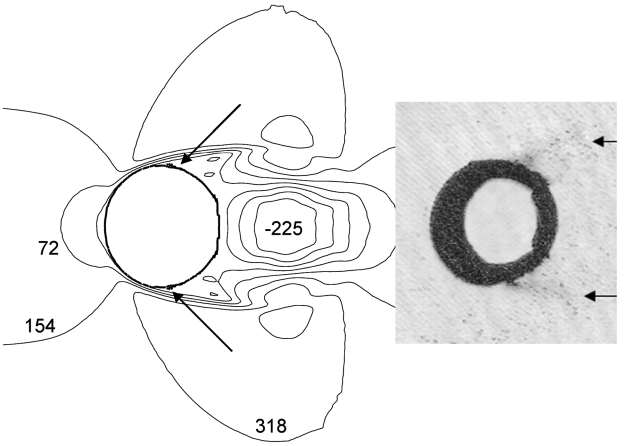

Fig. 8 Velocity contours (in m/s) in the *x* direction for incident shock wave Mach number 1.47 at 80 μs after impact. Experimental interferogram taken from [11].

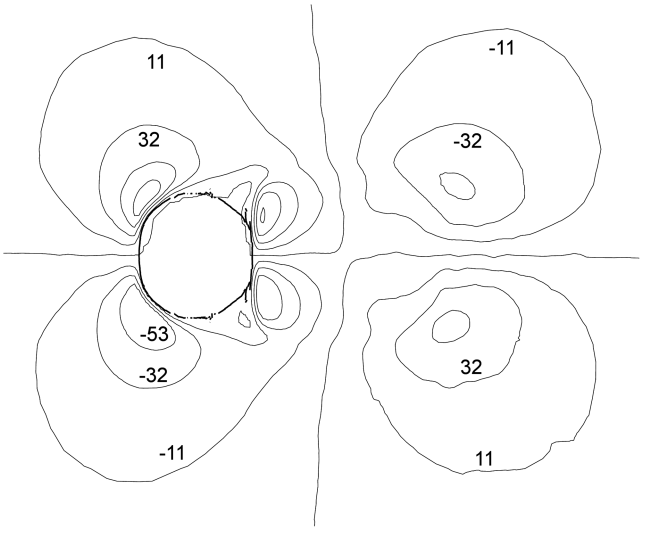

Fig. 7 Velocity contours (in m/s) in the *y* direction for incident shock wave Mach number 1.3 at 300 μs after impact.

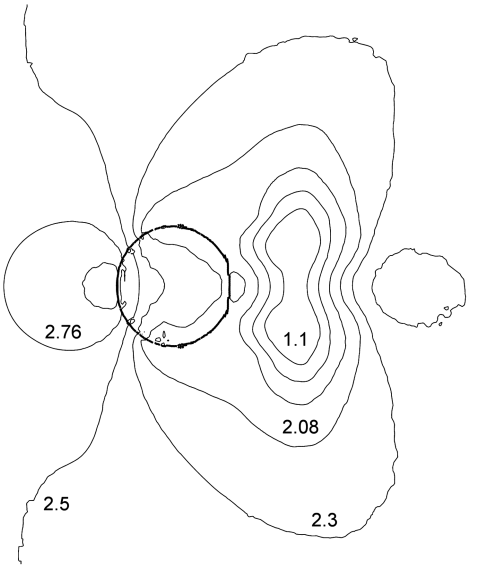

Fig. 9 Pressure contours (in bar) for incident shock wave Mach number 1.47 at 80 μs after impact.

propagation upstream. With progressing time, the incident and reflected shock waves have propagated further away from the water column. At the rear of the water column, a pair of vortices has formed. At the front of the water column, a high-density region is observable in both the numerical results and in the experimental findings. At 105 μs after the incident shock wave impacted on the water column, the first signs of the fragmentation process become visible, as shown in Fig. 4, which describes the velocity contours in the x direction. At the sides of the water column where the boundary layer separates, a small ligament is seen. This ligament marks the initiation of fragmentation; its behavior is typical to a stripping-type droplet breakup in a shearing mode. The two vortices are still present behind the water column and seem to remain at the same position they had in the previous time step. The simulated flow structure is similar to that observed in experimental results. Moving forward to Fig. 5, where the prevailing flowfield at 200 μs after impact is shown, one clearly notices that the water column shows signs of deformation. Its aspect ratio (width divided by length) is 1.08, which is similar to the experimental results given in [12] and shown next to the numerical simulation. On the rear part of the water column, on both sides, there is an area of low velocity that corresponds to the micromist dark region shown in the recorded interferograms available in [17,18]. In addition, it can be seen that the rear of the water column becomes flat, with ligaments forming. The ligaments are produced by the twin vortices shown in previous figures. Here, these vortices have started a secondary shearing location on the rear of the water column. One should also notice that there are no piercing Rayleigh–Taylor (RT) waves at the front of the water column, which appears smooth and without any oscillations. The last results for this Mach number are those taken 300 μs after the incident shock wave hit the water

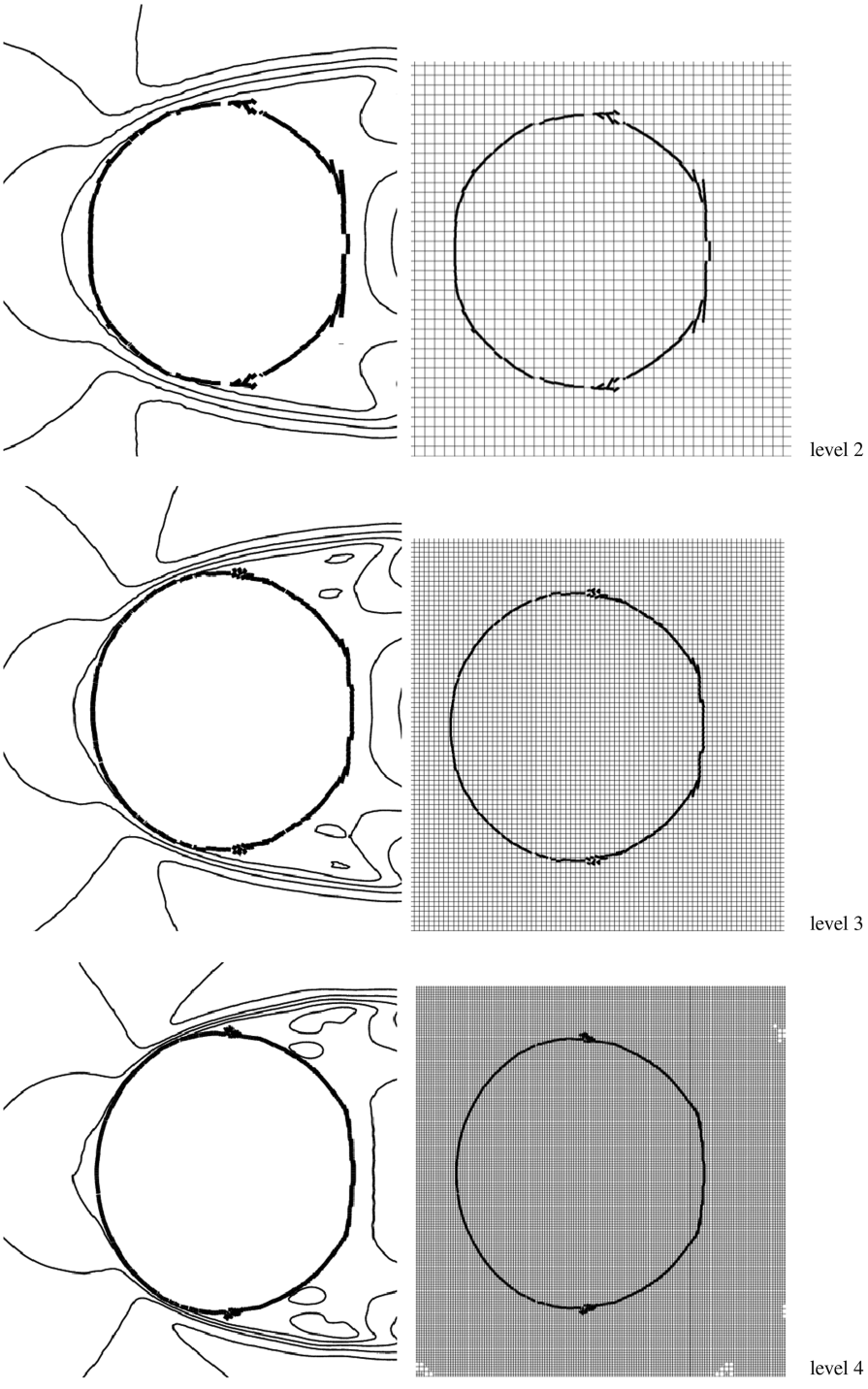

Fig. 10 Velocity contours in the x direction for incident shock wave Mach number 1.47 at 80 μs after impact for three different levels of grid refinement.

column; shown in Fig. 6. Here, the water column is continuing its deformation while its front and rear surfaces become flatter relative to the previous time step of 200 μs. The shape of the water column is similar to that obtained in experiments reported in [17,18]. Now the vortex shedding behind the water column is not symmetric anymore, as is evident from Fig. 7 that shows velocity contours in the y direction. This kind of unsteady shedding is similar to the interferogram presented in [17,18], where the micromist location is not symmetrical. To the best of our knowledge, this is the first time that numerical results for this stage of fragmentation are given.

B. Results for Mach Number 1.47

Turning our attention to the second case, where the incident shock wave is of Mach number 1.47 and the water column diameter is 4.8 mm. Some experimental work and numerical results covering the initial stages of the interaction were reported in [11,15]. Therefore, we shall start inspecting the water column 80 μs after its collision with the incident shock wave. Results of the present computations for the velocity component in the x direction and pressure variations are shown in Figs. 8 and 9, respectively. At the considered time, the water column is deformed: its rear part is flattened, while its frontal surface is not as round as it was originally. Regions of high pressure appear at the rear surface of the water column due to the secondary reflected shock wave that, by now, moved further upstream. In addition, there exists a high-pressure region in front of the water column due to the flow stagnation there. These two high-pressure regions are the driving force of the water column's initial deformation. A pair of vortices is seen behind the water column similar to what was shown in the previous case. Careful observation of the water column sides indicates that the first ligaments appear. The simulated flowfield and ligaments have very good agreement with the experimental interferogram, shown in Fig. 8 (taken from [11]). The location of the ligaments on the sides of the water column corresponds well with the experiments and, from observing the velocity field shown in Fig. 8, one notices that these ligaments are located where the boundary layer separates from the water column. This supports our theory that, for this type of high-speed flow, the stripping breakup is actually a boundary-layer shearing mechanism. It should be noted that this onset of fragmentation is grid independent, as shown in Fig. 10, for three different levels of grid refinement. The refinement levels are based on an adaptive mesh refinement with two to four levels of refinement. Next to each velocity contour, the grid is shown. The number of cells across the water column diameter was 26, 52, and 104 for grid refinement levels of 2, 3, and 4, respectively. As can be clearly seen at 80 μs, results obtained for each of the three different grids displays the same sort of fragmentation and in the same region, in agreement with experimental findings reported in [11]. As expected, increasing the level of refinement increases the number of cells and resulted in a rounder water column shape.

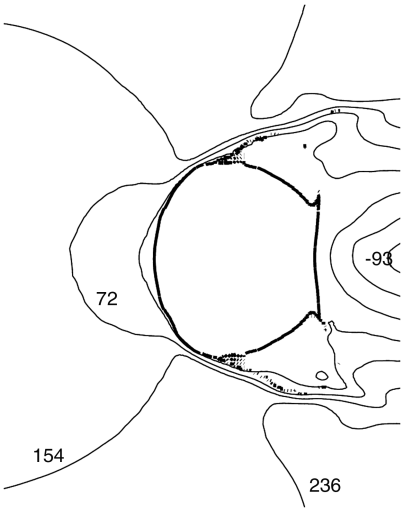

Fig. 11 Velocity contours (in m/s) in the x direction for incident shock wave Mach number 1.47 at 240 μs after impact.

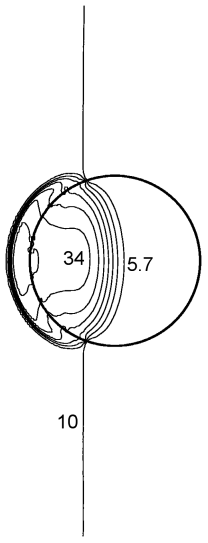

Fig. 12 Pressure contours (in bar) for incident shock wave Mach number 3 at 2 μs after impact.

At a later time, after the shock wave impacted on the water column (i.e., at 240 μs after the initial shock wave impingement), the diffracted shock wave around the water column is long gone, and a very clear deformation of the water column is visible in Fig. 11, where the velocity in the x direction is shown. The deformation of the water column is similar to that observed in interferograms available in [11]. The fishlike tail of the water column rear section might look unusual; this pattern is due to the rear vortices that shear the rear section of the water column. In [9,10], experimental results for a

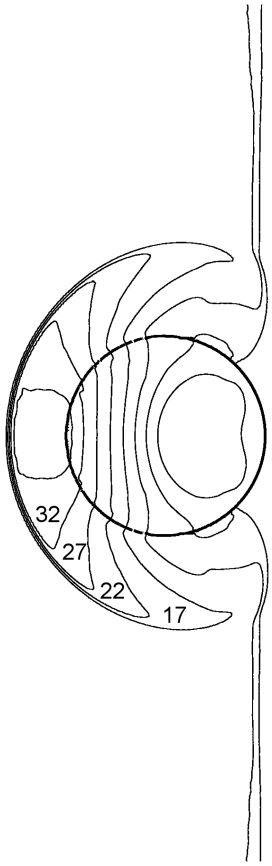

Fig. 13 Pressure contours (in bar) for incident shock wave Mach number 3 at 6 μs after impact.

sphere impinged by an incident shock wave, for which the Mach numbers were 1.3 and 3, respectively, exhibited a similar fishtail structure. Now that we have demonstrated that the current scheme yields good agreement with experimental findings, we shall turn our attention to the higher Mach number case, where $M = 3$.

C. Results for Mach Number 3

In this section, results for shock wave impingement ($M = 3$) on a 6.4-mm-diam water column are presented. Pressure contours at 2 μs after the incident shock wave hit the water column are shown in Fig. 12. Here, the reflected shock wave and the transmitted shock wave (inside the water column) are clearly visible. Because of the higher sound speed in water, the transmitted shock wave in the water column propagates faster than the incident shock wave. At this time, a small Mach stem appears at the intersection between the reflected and incident shock waves. Pressure contours at a later time (at 6 μs) are shown in Fig. 13. At this time, the transmitted shock wave inside the water column reflected back, resulting in a pressure gradient in the front of the water column. At the considered time, the incident shock wave just reached the rear of the water column while the refracted shock wave and the reflected shock wave are propagating toward each other on the rear part of the water column. Twelve microseconds after hitting the water column, the incident shock wave has completed its diffraction and passed the water column, as shown in Fig. 14. Now the shock wave tips that refracted over the water column meet behind the past obstacle. At this time, a high-pressure region exists in front of the water column due to the reflected shock wave. At the rear of the water column, the high-pressure region, created by interaction of the two parts of the refracted shock wave, begins to dissipate as the shock moves further downstream. At the considered time (12 μs), the water column still keeps its original shape.

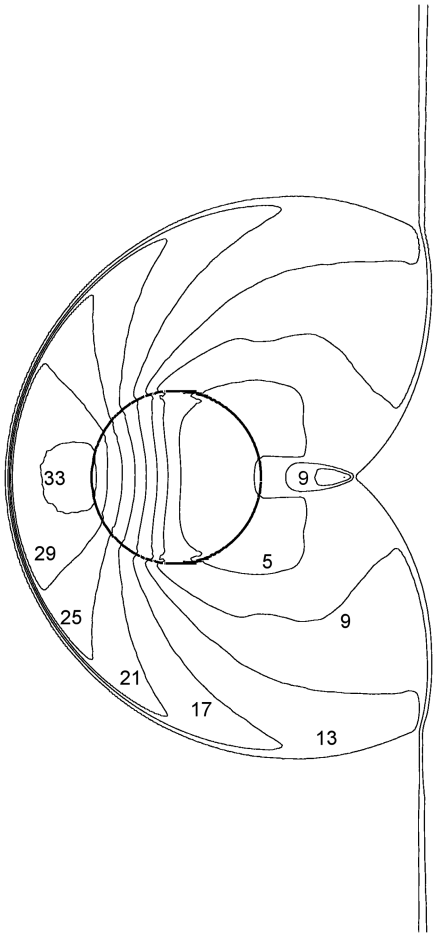

Fig. 14 Pressure contours (in bar) for incident shock wave Mach number 3 at 12 μs after impact.

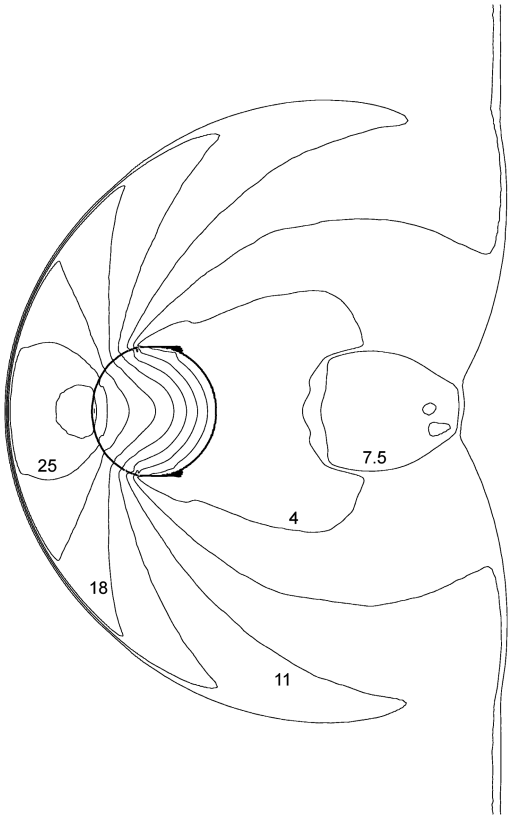

Fig. 15 Pressure contours (in bar) for incident shock wave Mach number 3 at 20 μs after impact.

Pressure contours at 20 μs after the initial impact of the incident shock wave on the water column are shown in Fig. 15. Now the incident shock wave has propagated further downstream than the reflected shock wave propagated upstream. The reflected shock wave and the stagnation flow it created imposed a high-pressure region on the frontal surface of the water column. In the considered time, the water column starts deforming and, at both of its sides, initial fragments are clearly visible. Based on the three different cases

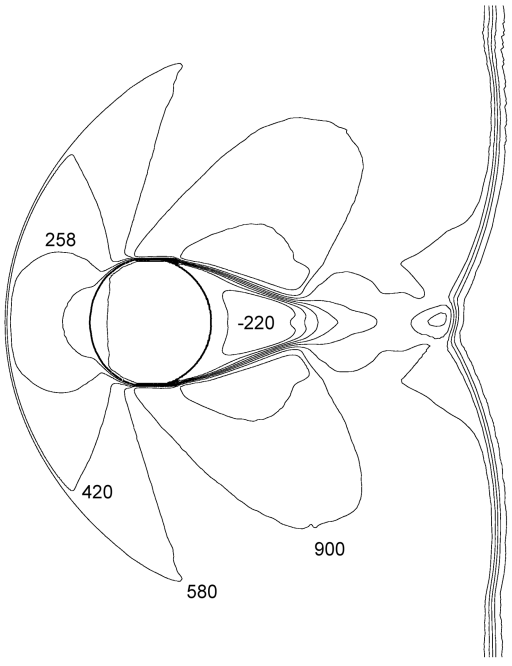

Fig. 16 Velocity contours (in m/s) in the x direction for incident shock wave Mach number 3 at 20 μs after impact.

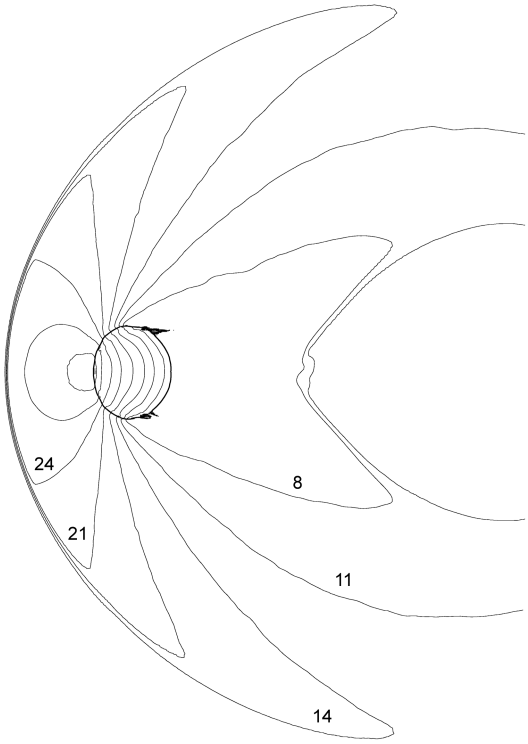

Fig. 17 Pressure contours (in bar) for incident shock wave Mach number 3 at 40 μs after impact.

where the incident shock wave Mach numbers were 1.3, 1.47, and 3, one can define a nondimensional time for initiation of fragmentation. Here, we define a nondimensional time t^*, $t^* = tu_2/d_0$ (where t is the time elapsed from the shock wave impingement, u_2 is the induced flow velocity behind the shock wave, and d_0 is the initial water column diameter). For values in the range of $t^* \approx 3$–4, the onset of fragmentation begins. The current results obtained at 20 μs fit this criterion. The reason for choosing a range rather than a single number is due to large variations in the incident shock wave Mach number and in the initial water column diameters. The fragmentation location is at the maximum diameter of the water column. In Fig. 16, velocity contours in the x direction are shown for $M = 3$. Here, a high shearing flow velocity is observed on both sides of the water column. This high velocity flattens the sides of the water column and shears small fragments from the water column. These fragments appear at the sides of the water column closer to its rear. It is apparent that, at this region, the extent of the shear flow is slightly widened as the flow

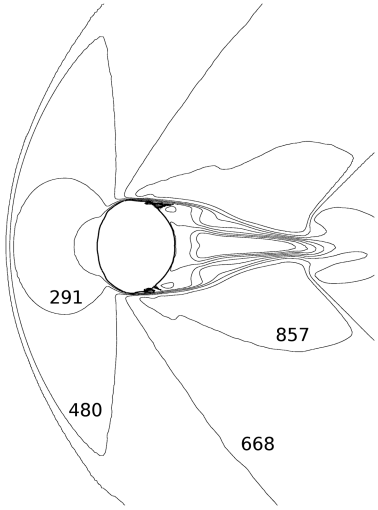

Fig. 18 Velocity contours (in m/s) in the x direction for incident shock wave Mach number 3 at 40 μs after impact.

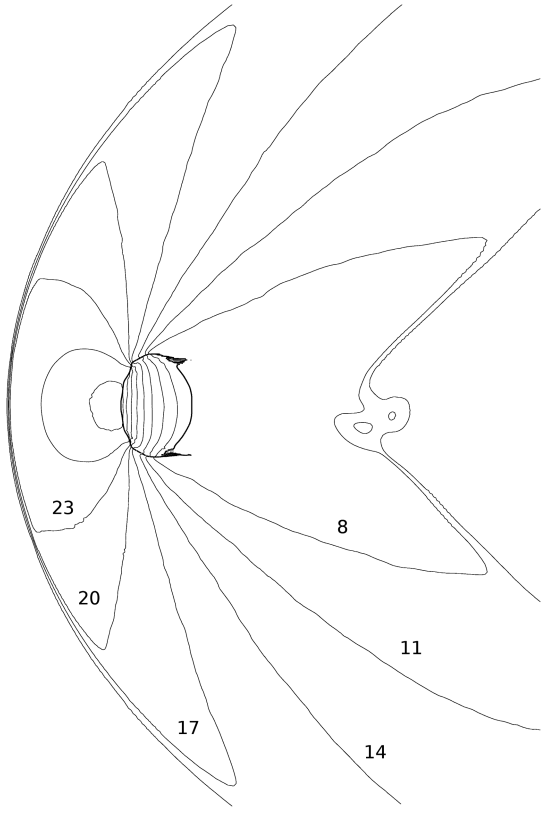

Fig. 19 Pressure contours (in bar) for incident shock wave Mach number 3 at 60 μs after impact.

moves downstream of the water column. As expected, a separate flow region exists behind the water column.

At 40 μs after the shock impact, the water column continues to deform, and now a noticeable pressure gradient exists all the way from the water column front and up to its rear. On both sides of the water column, clear signs of shearing breakup are visible: see in Fig. 17 and in Fig. 18, where the x component of the flow velocity contours are shown. In the velocity field (Fig. 18), a strong shear flow is seen on both sides of the water column; these shear flows cause the shearing breakup. In both Figs. 17 and 18, the front of the water column remains continuous, without any evidence of RT waves or oscillations. It appears that the high static and dynamic pressures that act on the frontal surface of the water column have flattened this part, while the rear surface retains most of its circular shape. The flow behind the rear part of the water column is oscillating, resulting in generating ligaments of different sizes on both sides of the water column. The last time step to be analyzed takes place at 60 μs after the initial impact of the incident shock wave on the water column. Pressure contours for this time are shown in Fig. 19. The water column continues its deformation. Its frontal surface is further flattened due to the high pressure prevailing on this surface. while its rear is still relatively round due to the lower pressure there. On both sides of the water column, the high-speed shear flow regions are clearly visible. The boundary-layer stripping is intensified, and ligaments on both sides of the water column are visible. The ligaments appearing on both sides of the water column have different sizes due to the nonsymmetrical vortex detachment from the water column.

IV. Conclusions

In the current paper, a fully conservative scheme that took into account subcell-sized particles, such as water ligaments, was employed for the first time. Applying this scheme, shock wave interaction with a water column for incident shock wave Mach numbers of 1.3, 1.47, and 3 was solved. In all three cases, it was possible to view the onset of fragmentation on the sides of the water

column: these appear at about $t^* \approx 3$–4. In addition, the deformation of the water column was analyzed, and its shape during deformation was similar to that obtained in experiments. Generally good agreement was obtained between the numerical results and experimental findings regarding the water column deformation and shock wave locations. Furthermore, for the cases presented here, no RT piercing waves were found. On the contrary, the main mechanism of the water column breakup was boundary-layer stripping due to the high-velocity shear flow and the slow moving and deforming water column.

References

[1] Wierzba, A., and Takayama, K., "Experimental Investigation Liquid Droplet Breakup in a Gas Stream," *Reports of the Institute of Fluid Science*, Vol. 53, 1987, pp. 1–99.

[2] Ranger, A. A., and Nicholls, J. A., "Aerodynamic Shattering of Liquid Drops," *AIAA Journal*, Vol. 7, No. 2, 1969, pp. 285–290. doi:10.2514/3.5087

[3] Ranger, A. A., and Nicholls, J. A., "Atomization of Liquid Droplets in a Convective Gas Stream," *International Journal of Heat and Mass Transfer*, Vol. 15, No. 6, 1972, pp. 1203–1211. doi:10.1016/0017-9310(72)90185-8

[4] Joseph, D. D., Belanger, J., and Beavers, G. S., "Breakup of a Liquid Drop Suddenly Exposed to a High-Speed Airstream," *International Journal of Multiphase Flow*, Vol. 25, Nos. 6–7, 1999, pp. 1263–1303. doi:10.1016/S0301-9322(99)00043-9

[5] Hirahara, H., and Kawahashi, M., "Experimental Investigation of Viscous Effects Upon a Breakup of Droplets in High-Speed Air Flow," *Experiments in Fluids*, Vol. 13, No. 6, 1992, pp. 423–428. doi:10.1007/BF00223250

[6] Krzeczkowski, S. A., "Measurement of Liquid Droplet Disintegration Mechanisms," *International Journal of Multiphase Flow*, Vol. 6, No. 3, 1980, pp. 227–239. doi:10.1016/0301-9322(80)90013-0

[7] Simpkins, P. G., and Bales, E. L., "Water Drop Response to Sudden Accelerations," *Journal of Fluid Mechanics*, Vol. 55, No. 4, 1972, pp. 629–639. doi:10.1017/S0022112072002058

[8] Yoshida, T., and Takayama, K., "Interaction of Liquid Droplets with Planar Shock Waves," *Journal of Fluids Engineering*, Vol. 112, No. 4, 1990, pp. 481–486. doi:10.1115/1.2909431

[9] Theofanous, T. G., and Li, G. J., "On the Physics of Aerobreakup," *Physics of Fluids*, Vol. 20, No. 5, 2008, Paper 052103. doi:10.1063/1.2907989

[10] Wierzba, A., and Takayama, K., "Experimental Investigation of the Aerodynamic Breakup of Liquid Drops," *AIAA Journal*, Vol. 26, No. 11, 1988, pp. 1329–1335. doi:10.2514/3.10044

[11] Igra, D., and Takayama, K., "Investigation of Aerodynamic Breakup of a Cylindrical Water Droplet," *Atomization and Sprays*, Vol. 11, No. 2, 2001, pp. 167–185.; also *Reports of the Institute of Fluid Science*, Vol. 11, 1999, pp. 123–134.

[12] Igra, D., and Takayama, K., "A Parametric Study of Water Column Deformation Resulting from Shock Wave Loading," *Atomization and Sprays*, Vol. 12, Nos. 5–6, 2002, pp. 577–591. doi:10.1615/AtomizSpr.v12.i56.20

[13] Abgrall, R., "How to Prevent Pressure Oscillations in Multicomponent Flow Calculations, A Quasi Conservative Approach," *Journal of Computational Physics*, Vol. 125, No. 1, 1996, pp. 150–160. doi:10.1006/jcph.1996.0085

[14] Shyue, K., "An Efficient Shock—Capturing Algorithm for Compressible Multicomponent Problems," *Journal of Computational Physics*, Vol. 142, No. 1, 1998, pp. 208–242. doi:10.1006/jcph.1998.5930

[15] Igra, D., and Takayama, K., "Numerical Simulation of Shock Wave Interaction with a Water Column," *Shock Waves*, Vol. 11, No. 3, 2001, pp. 219–228. doi:10.1007/PL00004077

[16] Igra, D., and Takayama, K., "A High Resolution Upwind Scheme for Multi-Component Flows," *International Journal for Numerical Methods in Fluids*, Vol. 38, No. 10, 2002, pp. 985–1007. doi:10.1002/fld.251

[17] Igra, D., and Takayama, K., "Experimental And Numerical Study Of The Initial Stages In The Interaction Process Between A Planar Shock Wave And A Water Column," *Proceedings of the 23rd Symposium on Shock Waves* [CD-ROM], Univ. of Texas at Arlington, Texas, 2001.

[18] Igra, D., and Takayama, K., "A Study of Shock Wave Loading on a Cylindrical Water Column," *Reports of the Institute of Fluid Science*, Vol. 13, 2001, pp. 19–36.

[19] Sethian, J. A., *Level Set Methods and Fast Marching Methods*, edited by P. O. Ciarlet, A. Iserles, R. V. Vohn, and M. H. Wright, Cambridge Univ. Press, New York, 1999.

[20] Sun, M., "A Unified Numerical Approach For Both Volume-Of-Fluid (VOF) and Two-Fluid Models: Basic Ideas and 1-D Tests" *International Journal for Numerical Methods in Fluids*, (submitted for publication).

[21] Sun, M., "Volume-Tracking of Subgrid Particles," *International Journal for Numerical Methods in Fluids* [online], 2010. doi:10.1002/fld.2331

[22] Nourgaliev, R. R., Dinh, T. N., and Theofanous, T. G., "Adaptive Characteristics-Based Matching for Compressible Multifluid Dynamics," *Journal of Computational Physics*, Vol. 213, No. 2, 2006, pp. 500–529. doi:10.1016/j.jcp.2005.08.028

[23] Chang, C. H., and Liou, M. S., "A Conservative Compressible Multifluid Model for Multiphase Flow: Shock-Interface Interaction Problems," 17th AIAA Computational Fluid Dynamics Conference, AIAA Paper 2005-5344, June 2005.

[24] Toro, E. F., Spruce, M., and Speares, W., "Restoration of the Contact Surface in the HLL-Riemann Solver," *Shock Waves*, Vol. 4, No. 1, 1994, pp. 25–34. doi:10.1007/BF01414629

[25] W, E., Engquist, W. E. B., Li, X., Ren, W., and Vanden-Eijnden, E., "Heterogeneous Multiscale Methods: A Review," *Communications in Computational Physics*, Vol. 2, No. 3, 2007, pp. 367–450.

X. Zhong
Associate Editor